Bio-Inspired Hierarchical Polymer Fiber-Carbon Nanotube Adhesives

*Zhuxia Rong, Yanmin Zhou, Bingan Chen, John Robertson, Walter Federle, Stephan Hofmann, Ullrich Steiner, and Pola Goldberg-Oppenheimer**

Natural adhesive systems, consisting of pads covered by dense assemblies of high aspect ratio branched adhesive setae, (**Figure 1**a) excel in terms of adhesive strength on nearly any surface. Facile contact release is achieved by spatulae at the seta tips that are inclined with respect to the setae axis, requiring a normal preload and shear to establish adhesive contact and enabling low-resistance contact release by peel-off. While technologically valuable, dense hierarchical fibrillar adhesives are difficult to manufacture and no scalable approaches yet exist to create the required spatulae asymmetry. Here we demonstrate the manufacture of biomimetic hierarchical nanostructures based on polymer micro-pillar arrays topped with densely packed, vertically aligned carbon nanotubes (CNTs), which closely resemble gecko toe-pads. A permanent spatula-like asymmetry is introduced into the CNT assembly during a first adhesion-release cycle consisting of a normal preload and a shear motion. The shear adhesion forces of these deformed hierarchical CNTs/polymer pillar arrays on smooth and rough surfaces were found to be considerably higher than those of non-structured (i.e., plain) CNT forests, caused by the conformal attachment of the multilevel adhesive elements to the coarse surface topography, energy dissipation during the deformation of the polymer pillars and the increased contact area provided by the inclined CNTs.

Exploitation of the naturally optimized design principles of controllable attachment found in biological systems is highly desirable for synthetic adhesives. If successful, such sophisticated biomimetic adhesives would enable a new platform for a variety of applications, ranging from the micromanipulation in production processes, to microelectronics, robotics and biomedicine. Strong, rapid and robust adhesion mediated by gecko toe pads relies on the conformal contact of a finely structured adhesive area to any surface profile, while maintaining structural integrity and wear-resistance.[1–3] While highly efficient in a large number of biological organisms, the biomimetic replication of the "gecko effect" is difficult because of the complex geometry of the adhesive surface and its required hierarchical structure.

The toe-pads of geckos consist of millions of branched adhesive setae (Figure 1a), which are arranged in a grid-like pattern on the ventral surface of each scansor, branching out into hundreds of nanometer-sized spatular tips (ca. 200 nm wide), allowing them to deform and adhere to nearly any surface.[4] Gecko toe-pads consist of β-keratin (elastic modulus E = 1–3 GPa).[5,6] The intimate contact with surfaces of any roughness[7,8] gives rise to significant van der Waals (vdW) forces,[9] and their asymmetric structure allows controlled attachment and detachment during locomotion.[10,11]

Although considerable progress has been made in mimicking fibrillar adhesives by utilizing nanofabrication routes including photo and electron-beam lithography,[12–14] micro molding[15–20] and CNT growth,[21–25] only some of the benchmark properties of natural fibrillar adhesives (e.g., anisotropic attachment, vdW adhesion, low detachment force, self-cleaning, anti-self matting, compliance and wear resistance) have been achieved to date. Only few biomimetic adhesives have been produced with a hierarchical structure similar to gecko setae. However, recent work on polymer-based nanostructures has demonstrated that hierarchical design is essential for achieving good adhesion to rough surfaces.[16] This is due to the ability of hierarchical structures to compensate for surface roughness on different length scales.

The creation of a hierarchical fibrillar adhesive is challenging. Synthetic polymeric multilevel structures are mechanically weak, which limits the potentially obtainable aspect ratio.[26,27] CNTs, on the other hand, are promising materials for the manufacture of fibrillar adhesives because of their small tip size, high aspect ratio and high modulus, giving a combination of compliance, insensitivity to tip geometry, wear resistance and resistance to contamination. While there are several reports on macroscopic arrays of vertically aligned carbon nanotube forests (CNTFs) which combine high mechanical strength with sufficient flexibility to achieve high shear forces relative to the normal adhesion forces,[22,28,29] there is also a large, non-understood variation in the reported force values. The shear adhesion of CNTFs varies significantly with the length, density and the number of layers of nanotubes. The high shear forces of CNTFs also often require a large preload and adhesion is affected by the permanent deformation under loading. CNTFs have been previously transferred from the surface on which

Dr. Z. Rong, Prof U. Steiner
Department of Physics
University of Cambridge
Cambridge, CB3 0HE, UK
B. Chen, Prof. J. Robertson, Dr. S. Hofmann
Department of Engineering
University of Cambridge
Cambridge, CB3 0FA, UK
Y. Zhou, Dr. W. Federle
Department of Zoology
University of Cambridge
Cambridge, CB2 3EJ, UK
Dr. P. Goldberg-Oppenheimer
Department of Chemical Engineering
University of Birmingham
Birmingham, B15 2TT, UK
E-mail: p.goldbergoppenheimer@bham.ac.uk

DOI: 10.1002/adma.201304601

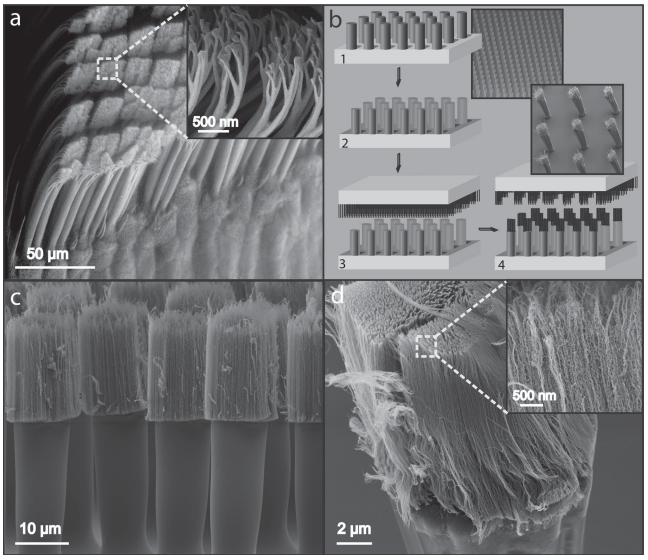

Figure 1. (a) SEM image of a gecko toe pad showing hierarchically organized setae that terminate in thousands of nanoscale spatulae (inset).[1] (b) Schematic illustration of the fabrication process: starting with (1) the photolithographic fabrication of an SU8 pillar arrays, the resulting pillar-array is (2) coated with an adhesive, followed (3) by imprinting a CNTF onto the SU8 pillars which after lift-off transfers the CNTs onto the SU8 pillars. (c) Side-on SEM view of polymer pillars tipped with CNTs. (d) Magnification of one individual pillar.

they were catalyzed onto planar polymer substrates,[22,29] but attempts have rarely been made to combine CNTFs with other structured materials to create a multi-level hierarchical design. Also, an artificial structure that matches the gecko toe-pads in terms of reversible adhesion performance, robustness and durability has yet to be reported.

Here, hierarchical gecko-inspired structures were fabricated by gluing CNTF onto a square array of SU8 pillars. Stiff SU8 epoxy (E = 4 GPa) was chosen as material because of its mechanical properties that are similar to β-keratin. Vertically oriented multi-walled CNTs with a site density in the range of 7% (measured by the weight-gain method),[30,31] an average diameter of 20 nm and a height of 20 µm were grown by a chemical vapor deposition (CVD) process (see Experimental for details). Pillar arrays (PAs) with a range of aspect ratios f (height/diameter) were fabricated (see Supporting Information, Figure S1). A SEM micrograph of a SU8 PA with f = 10 is shown in the inset of Figure 1b. A thin conformal layer of polymer glue (poly vinyl acetate, PVAc) was subsequently applied on the pillar array and a CNTF on a silicon substrate was brought in contact with the pillar tips, followed by annealing at 100 °C (above the glass transition temperature PVAc of $T_g \approx 35$ °C) and an applied pressure of 5 MPa. A careful optimization of the compression pressure during annealing was crucial because of the delicate balance of incomplete CNTs transfer and the deformation of the SU8 PA. Quenching the assembly to ambient temperatures and lifting off the substrate yielded SU8 pillar arrays tipped with CNTs.

High fidelity HPAs with dimensions similar to those of gecko toe-pads were fabricated over large surface areas (1 cm × 1 cm) (Figure 1c). The magnified image of one individual column (f = 10) reveals a dense array of CNTs (Figure 1d), which are permanently grafted onto the pillar top-surface. To test the adhesion performance of the HPA surfaces, we used a force measurement setup with a two-axis force sensor and feedback control of normal load (**Figure 2**a).[32] Although typically used for studying adhesion of insects, this setup has only rarely been employed for measuring the adhesive properties of biomimetic structures. Previous studies on bio-inspired fibrillar adhesives used a range of testing methodologies.[33–38] Most of these make use of a customized apparatus with a uniaxial force sensor, which complicates the recording and analysis of the adhesion versus preload data. The setup of Figure 2a enables a greater degree of control during the shear force measurement, where a preload-slide retract movement is performed using a spherical probe and shear force is measured while the probe is sliding over the sample surface and the normal force is maintained at a constant level.

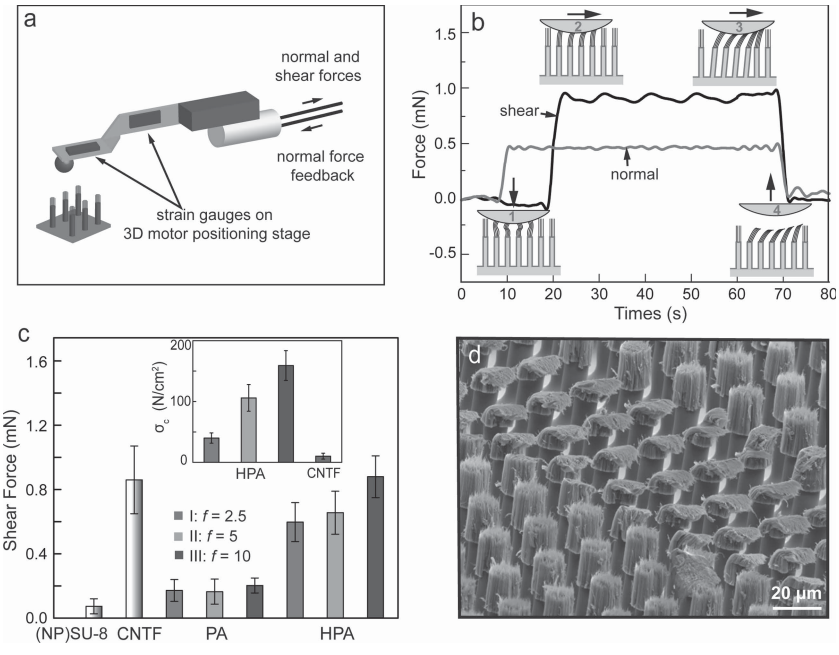

Figure 2. Adhesion performance of hierarchical pillar arrays (HPAs). (a) Schematic illustration of the experimental setup used to measure shear and normal forces of the HPAs.[32] (b) Representative curve of shear (black) and normal (grey) forces versus time for a HPA with f = 10 and a probe speed of 100 µm s^{-1}. The insets depict the four typical steps during the force measurement process. (c) Shear forces of PAs and HPAs of three different aspect ratios in comparison to the reference substrates of non-patterned SU8 and a CNTF sheared against a smooth probe. The insets show the normalized shear stress σ_c of HPAs compared to the CNTF. (d) SEM micrograph of the morphological change in the HPA structure caused by the shear adhesion measurements, showing the imprint of the probe surface.

Adv. Mater. **2013**,
DOI: 10.1002/adma.201304601

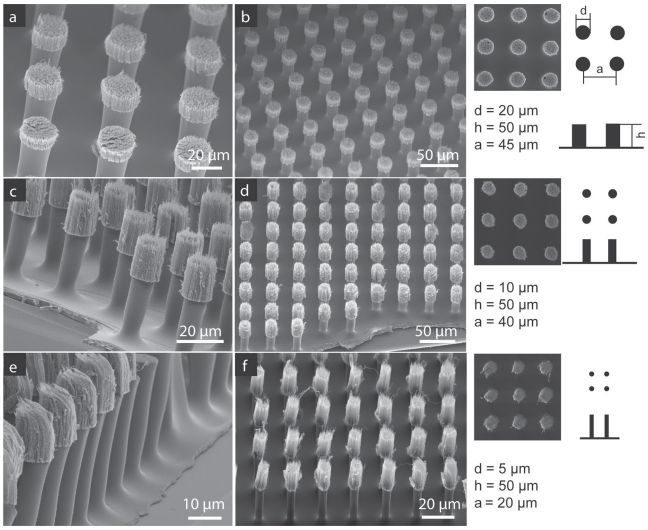

Figure 3. SEM images of HPAs with different structure dimensions (a, b) HPA-I ($d = 20$ µm, $a = 45$ µm, $\phi = 15.5\%$), (c, d) HPA-II ($d = 10$ µm, $a = 40$ µm, $\phi = 4.9\%$), (e, f) HPA-III ($d = 5$ µm, $a = 20$ µm, $\phi = 4.9\%$).

A representative force versus time curve for a HPA surface with $f = 10$ is shown in Figure 2b, depicting a typical load-displacement measurement cycle consisting of the initial preload (1), sliding/shearing (2 and 3), and retraction (4) steps (Figure 2b, insets). Reproducible force curves were obtained under the preload force of 0.5 mN for all measurements in this study. While a much higher preload caused structural failure of the SU8 pillars, insufficient preloads considerably increased noise in the measurements. In Step 1, the 20 µm high CNTs on top of the PAs were subjected to the preload of 0.5 mN. Sliding the probe triggered an alignment of CNTs in the shear direction (Step 2) causing a marked increase in friction force (Figure 2b). Two modes of HPA deformation can occur: (i) shear deformation of the CNTs (Step 2) and (ii) bending of the SU8 columns (Step 3). Unloading the probe resets normal and shear forces (Step 4).

Shear adhesion of HPAs with $f = 2.5$, 5 and 10, and pillar area coverage of $\phi = 15.5\%$, 4.9% and 4.9%, respectively (**Figure 3**), were measured against a smooth surface. Figure 2c shows the measured shear force F for the non-patterned SU8 surface, a pure CNTF substrate, simple SU8 pillar arrays (PAs) and hierarchical CNTF-SU8 arrays (HPAs) of three different aspect ratios. The decoration of the polymer pillars with CNTs resulted in a more than threefold increase in shear force (Figure 2c). The shear force supported by the HPAs of identical pillar area coverage $\phi = 4.9\%$ was higher for HPA-III with $f = 10$ compared to the lower aspect ratio HPA-II with $f = 5$. This implies that SU8 pillars undergo elastic deformation, thereby contributing to the increase in shear force. Moreover, pillar arrays with a small aspect ratio of $f = 2.5$ exhibited a similar shear stress as the arrays with $f = 5$, despite their more than three times higher pillar area coverage ($\phi = 15.5\%$ and 4.9%, respectively). Large pillar area coverage is likely required to compensate the contact area reduction due to the low aspect ratio SU8 pillars (less elastic deformation).

An increased adhesion has been demonstrated for high aspect ratio polymer patterns.[38] Although in the hierarchical structures the base-level pillars are capable of providing more compliance to the substrate, the relative contact area is reduced in comparison with the unstructured continuous CNTF. A spherical indenter, however, exhibits a larger contact area with compliant arrays (i.e., it is in contact with a larger number of pillars), which compensates for the decreased tip contact during shear adhesion compared to a continuous forest.

The maximum shear force of 0.88 ± 0.13 mN was obtained on the HPA with the highest aspect ratio $f = 10$. The apparent contact area A_0 between the probe and the HPA-covered surface was estimated from the SEM micrographs after shear adhesion measurements (Figure 2d and Figure S2). This yields a shear stress of 7.8 ± 1.2 N/cm^2 for the $f = 10$ HPA. While the maximum shear force of the $f = 10$ HPA is comparable to that of CNTF, it has a nanotube area coverage of less than 5%. The normalized shear stress σ_c plotted in the inset of Figure 2c therefore emphasizes the benefit of the hierarchically structured surface. Similar shear forces were observed when measuring HPAs with hydrophobic (Figure S3) and hydrophilic surfaces. This supports the assumption that the van der Waals forces dominate the adhesion between the carbon nanotubes and the probe surface.[9] Furthermore, since the CNTF was reversed during the fabrication process, the shear forces were measured from the bottom of the carbon nanotube arrays. Note that only a negligible normal adhesion force of HPA-covered surfaces was detected (i.e., when measuring in a load-retract cycle, see Figure S4), which was mostly indistinguishable from the force curve and screened by the noise. This may be explained by the small contact area of vertical CNT tips and by relatively low packing density and reduced area coverage of the HPA surfaces.

The morphological difference between the sheared and non-sheared HPA-covered areas, as shown in Figure 2d, reveals that while the polymer pillars restore their original pre-measurement configuration, CNTs are plastically deformed along the shear direction, which creates asymmetric spatula-like hairs. This post-measurement configuration implies an increased effective contact area provided by the CNT sidewalls, which appears to be beneficial in further attachment-detachment cycles as discussed further below.

To test whether the hierarchical pillar geometry also leads to improved shear adhesion on rough surfaces, shear forces of HPAs in contact with sub-micron rough surfaces were measured. While most natural surfaces contain roughness on many length scales, little attention has been paid to the effect of roughness on the adhesion properties of biological and biomimetic adhesives. Recent studies have demonstrated that roughness can significantly affect the performance of gecko[39] and synthetic biomimetic adhesives.[16,40,41]

Rough surfaces were prepared by chemical etching of a sphere probe. This yielded a surface roughness on a range of length scales, from ~100 µm down to ~100 nm (SI, Figure S5). An AFM measurement of a 100 µm^2 area yielded an average of height fluctuations of R_a = 200 nm. The SEM images of Figure S5 show additional structure on the ~10 µm and ~100 µm length scale that are not captured in this R_a-value, but which are likely to have an effect on the adhesion measurements, allowing the HPA to conform to the height fluctuations.

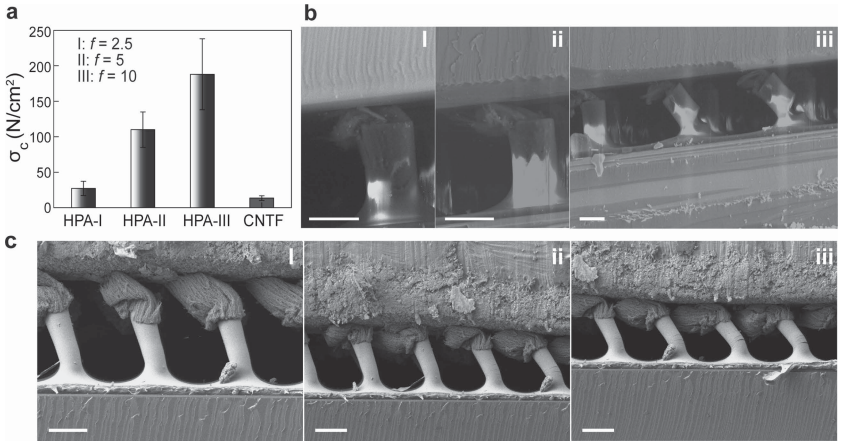

Figure 4. (a) Normalized shear stress σ_c of HPAs of three different aspect ratios compared to a CNTF measured against the rough surface with an average surface roughness of R_a = 200 nm. Shear forces were measured under a normal force of 0.5 mN and a probe speed of 100 µm s^{-1}. In-situ SEM images of HPAs under a constant normal load at different shear stages against a smooth (b) and a rough (c) surface. The scale bars are 20 µm and 10 µm, respectively.

The HPA-covered surface with f = 10 showed a shear stress of σ_c = 185±50 N/cm^2 (**Figure 4**a) normalized to the actual contact area, which is higher by nearly one order of magnitude compared to the pure CNTF substrate. (The shear force of the HPAs with f = 10 on the rough surface is comparable to the CNTF reference (Figure S6). The HPA compliance thus compensates the decrease in contact area of the CNTF substrate.

In-situ SEM characterization with an integrated tension stage was used to study qualitatively the morphological adaptation of HPAs during shear on both smooth (Figure 4b) and rough (Figure 4c) surfaces. When sheared against a smooth substrate, HPAs initially formed contacts with their CNTs tips to the surface, and then tilted in the shear direction to adhere with their side walls (Figure 4b i-ii). Further shear fractured the SU8 pillars close to their base (Figure 4b iii). This confirms the strong connection of CNTs to the SU8 pillars. This result also implies that the lower aspect ratio SU8 pillars do not play a substantial role in improving adhesion. Sequential SEM images of higher aspect ratio HPAs sheared against rough surfaces revealed similar initial adhesion morphologies of the HPAs with initial tip contacts and CNTs tilted in the shear direction. However, strong shear resulted in additional bending of the SU8 micro-pillars (Figure 4c iii) and no fracture of the SU8 pillars was observed for the comparable stage in Figure 4b iii, which indicates a greater compliance for high aspect ratio SU8 pillars.

These results provide a possible explanation for the increased shear stress measured with the f = 10 HPAs in Figure 4a, compared to the inset of Figure 2c, providing a rationalization for the benefit of compliant structures. While providing information of the morphological adaptation under shear, in-situ SEM does not allow sufficiently accurate force measurements. In-situ and ex-situ measurements were therefore combined.

These measurements suggest an adhesion mechanism for the hierarchical surface, resulting from a competition between adhesion energy and elastic deformation. The structural hierarchy equips the surface with the flexibility that is required to make contact with uneven surfaces. While the polymer pillars provide adaptability *via* bending deformation, the CNTs are able to deform around surface irregularities, without storing too much elastic energy, thereby increasing contact area.

The in-situ SEM observations show a shear-induced change in contact geometry by bending of the CNTs, enabling a greater side contact area and an increased shear adhesion. This formation of a side contact of nanotubes upon shear has been shown to result in an enhanced adhesion force of the continuous CNTs.[28] The shear-induced bending of the base pillars enhances this effect. Bending is also aided by the shear load applied to individual CNTs as the structured sample is sheared.[42,43] This leads to a decreased loading angle between the CNTs bundle and the surface, increasing the force along the direction of shear. Thus, the reduced stiffness of the high aspect ratio hierarchical structure facilitates a considerable shear enhancement due to the additionally increased contact area which extends the maximum displacement before detachment occurs, allowing the CNTs to maintain contact and leading to higher interfacial shear strength.

Note that while SU8 was chosen for its high stiffness, it is more brittle than β-keratin. Stiff materials are only beneficial in combination with high aspect ratios, and for low aspect ratio structures, soft materials are preferable. Spolenak et al. suggested that adhesion to rough surfaces requires a minimum elastic adaptability of a fiber structure.[44] The energetics of contact formation requires that the elastic strain energy stored in the material during contact is lower than the work of adhesion. These requirements can be met by setting an upper limit of ~1 MPa on the effective modulus of the fiber structure. To avoid buckling instabilities, the authors consider a fiber array that meets the substrate at an angle and is therefore stressed by bending. Using Persson's result[45] $E_{\mathrm{eff}} = CE\phi/4\pi f^2$, where C is a geometrical factor of the order of 10, E is the elastic modulus of the material, f is the fiber aspect ratio, and ϕ is the area fraction of fibers, an upper bound on the Young's modulus of the fiber material can be calculated. In our case f = 10, resulting in $E_{eff} = 4 \times 10^{-4}\ E$. This implies the elastic modulus of the SU-8 pillars is reduced from the material's bulk elastic modulus of E = 4 GPa to E_{eff} = 1.6 MPa, which lies close to the limit defined by Spolenak, i.e., is comparable to rubber and only slightly higher than biological adhesives. Nevertheless, it is important to mention that the simultaneous optimization of pillar material in terms of its stiffness and fracture toughness is therefore likely to further improve the shear-adhesion performance of HPAs.

The structural integrity and durability of HPA surfaces were investigated by oscillatory shear adhesion measurements (with each hierarchical pillar subject to attachment and detachment as the probe slides along) over 25 cycles, as shown in **Figure 5**a. Following the deformation of the CNTs after the first shear movement, a movement in the opposite direction was performed (Figure 5a, left inset). Interestingly, a symmetric shear force curve

Adv. Mater. **2013**,
DOI: 10.1002/adma.201304601

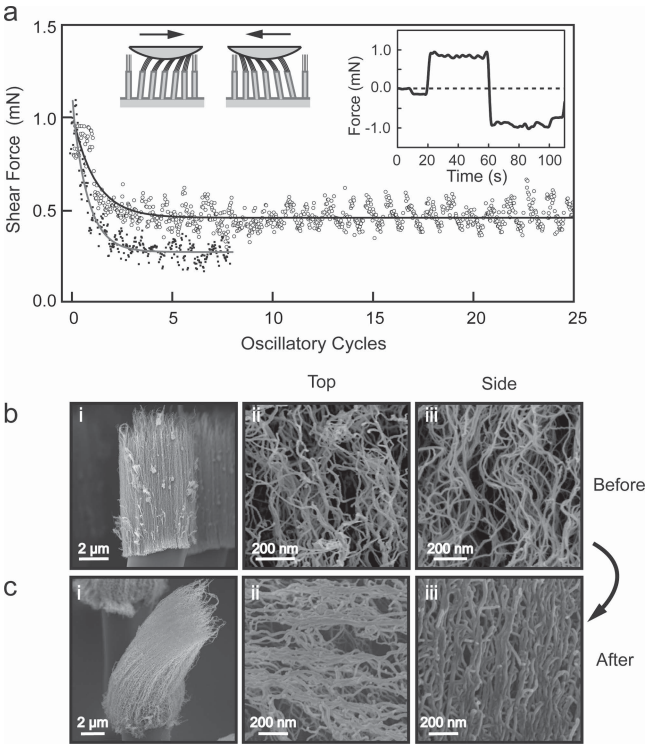

Figure 5. (a) Shear force measurements of a HPA with $f = 10$ (open circles) over 25 oscillatory cycles compared with a CNTF (filled circles) over 8 cycles (trend line is to guide the eye). The inset on the left-hand side depicts the structural change in HPAs during the oscillatory measurements. A symmetric shear force curve observed for each cycle is shown in the right-hand side inset. SEM images of the morphological changes (i-iii) of the CNTs grafted on top of polymer pillars prior to (b) and following (c) the shear adhesion measurements.

was observed for each cycle (Figure 5a, right inset). The deformed hierarchical structures produced a shear force comparable to that in the initial upright state. The plastic deformation of the CNTs on top of SU8 pillars resulted in a shear force that decreased by a factor of two after the initial shear cycle and then remained constant over the following 23 cycles, in contrast to a decrease in shear force by a factor of four of the CNTF after two cycles (Figure 5a). Since the shear adhesion of CNTF arises mainly from the tip contact, compared to the both tip and side contact contributions for the HPAs, the repeated stretching of the tip entanglements leads to a faster degradation of adhesion forces using the CNTFs.

To understand the robustness of HPA surfaces, we examined the morphologies of CNTs before and after the initial shear cycle. The CNTs on polymer pillars consisted of loosely packed bundles (Figure 5b iii) with randomly entangled tips (Figure 5b ii). The applied shear force caused the vertical nanotube bundles to tilt in the shear direction (Figure 5c i). This stretches the entangled CNT-web in the lateral (Figure 5c ii) and vertical (Figure 5c iii) direction, allowing CNT sidewall adhesion and higher shear forces. After 25 shear-cycles, we observed deformation of CNTs due to bending and torsional load, and full CNT collapse in some contact areas (Figure S7). These post-measurement morphologies of HPA surfaces reveal that repeated shearing results in irreversible plastic deformation of nanotubes, evident by the deteriorated shear adhesion.

In conclusion, we have established an approach for the fabrication of hierarchical pillar arrays consisting of micrometer-sized polymer setae covered by CNTs that play the role of spatulae, mimicking the fibrillar adhesive surfaces of geckos, spiders, and insects. We have tested the effect of the hierarchical arrangement of CNTs on arrays of SU8 pillars of different aspect ratio and area coverage on the shear forces on smooth and rough surfaces. The shear stress of HPAs on rough surfaces was nine times higher than for a pure CNTF substrate. This is a direct outcome of the structural hierarchy of HPAs, which enables enhanced conformal attachment of the adhesive elements to the rough surface topography. Our study provides a proof-of-principle that clearly shows that hierarchically engineered structures based on polymer and CNTs are a viable approach for the design of biomimetic fibrillar adhesives. Further optimization of structural parameters and the used polymer material is likely to improve the strong and repeatable adhesion of HPA-structured materials.

Experimental Section

Lithographic Fabrication of SU8 Pillar Arrays: SU8 microstructures were manufactured by photolithographic patterning of SU8 on silicon wafers using a mask aligner (Suss Microtex MJB4). The SU8 pillars were arranged in a square lattice with center-to-center spacing of $a = 20$ μm, 40 μm, 45 μm, diameters of $d = 5$ μm, 10 μm, 20 μm and a height of $h = 50$ μm, yielding aspect ratios of 2.5, 5, 10, and pillar area coverage of 15.5%, 4.9% and 4.9% respectively. The overall area covered by SU8 pillars was 1×1 cm^2. A Hoya UV34 filter was used to cut off wavelengths below 340 nm during the irradiation step. This yielded pillar arrays with aspect ratios of up to $f = 10$. Pillars with even higher aspect ratios ($f = 15$) could be fabricated with this method (see Supporting Information), but were found to be mechanically unstable. Further process details are provided in the Supporting Information.

CNTF Fabrication: Vertically aligned multi-walled carbon nanotube forests (CNTFs) were grown by thermal chemical vapor deposition at 650 °C in 200:500:10 sccm Ar:H_2:C_2H_2 at atmospheric pressure, from sputtered Al_2O_3 (10 nm)/Fe (1 nm) films supported on Si wafer substrates.[25,46] The samples were transferred in air between the catalyst layer depositions before being loaded into the 2″ diameter quartz tubing of the CVD furnace (Carbolite). Subsequently, the samples were heated up to 650 °C under a 1000 sccm flow of Ar, annealed for 3 min in 200:500 sccm Ar/H_2, and then 10 sccm of C_2H_2 were added to start CNT growth. The CNT length (20 μm) was controlled by the growth time of 3 min. The samples were cooled to room temperature in Ar atmosphere.

Transfer of CNTs onto SU8 Pillar Arrays: Polyvinyl acetate (PVAc) was spin-cast onto the substrate covered by SU8 pillars, forming a thin layer on top of the pillars. The vertically aligned CNTs were transferred onto the SU8 pillars by an imprinting process. The SU8 pillars were contacted by the CNTF (which was supported by a Si substrate) and annealed at 100 °C at a pressure of 5 MPa for 15 min. Following a quench to the room temperature (resulting in the solidification of the PVAc), the Si substrate was manually lifted off, and CNTs were successfully transferred from the Si substrate onto the SU8 pillars.

Adhesion Measurement: Adhesive forces were measured using a force transducer made of a folded metal bending beam mounted on a XYZ motor positioning stage. The motor movements and force recording were synchronized by a Lab-VIEW program that included a normal force feedback mechanism. The force sensors were calibrated for different lever arm lengths by applying milligram weights and defined displacements. The force sensor had a stiffness of 40.9 N/m and a resolution of less than 0.1 mN.

Shear forces were measured in sliding experiments. A glass sphere of 1 mm diameter was glued to the free end of the bending beam

and used as a smooth probe. The glass sphere was exposed to a hexamethyldisilazane (HMDS) vapor at 100 °C for 16 h to render the glass hydrophobic. Flat glass treated in this way had a contact angle with water of $\theta = 110°$. A stainless steel sphere of 1.5 mm diameter was etched in 6M H_2SO_4 for 3 h to induce a sub-micrometer roughness. The surface morphology of the sphere was investigated by SEM and AFM (Figure S5). The surface roughness was RMS = 250 nm, R_a = 200 nm as measured by AFM. Glued to the cantilever, this sphere served as a rough probe.

Shear force measurements against smooth and rough probes were performed using the same protocol. The samples were brought into contact with the spherical probe in the normal direction for 10 s with a normal force of 0.5 mN, followed by a lateral displacement of the probe and final retraction from the measured surface. The sliding motion was performed for 40 s with a velocity of 100 μm s^{-1} covering a distance of 4 mm while the normal force was kept constant by the force feedback loop. After sliding, the probe was put on hold for 10 s followed by the retraction motion for 10 s with a velocity of 100 μm s^{-1}.

Oscillation force measurements were performed by repeated shear at a speed of 100 μm s^{-1} for 25 cycles using the smooth glass probe. Normal adhesion forces were measured using the indentation procedure without shear. The probe typically indented the sample surface with a fixed normal force of 0.5 mN for 40 s and then retracted until no force could be measured.

In-Situ SEM Imaging: In-situ observation of morphology change under shear was performed using a tension/compression stage mounted into the SEM (Philips XL 30 FEG) chamber. The piezoelectric actuated stage was utilized for precise sample positioning and it was controlled using LabVIEW Software.

Supporting Information

Supporting Information is available from the Wiley Online Library or from the author.

Acknowledgements

U.S. and W.F. thank the Cambridge Overseas Trust (to Z.R. and Y.Z.) and the Biotechnology and Biological Sciences Research Council (BBSRC, BB/I008667/1). S.H. acknowledges funding from ERC grant InsituNANO (project no. 279342) and P.G.O. and J.R. the funding from EC project 'Grafol'. JJ Rickard is kindly acknowledged for his advice regarding the in-situ SEM imaging.

Received: September 12, 2013
Revised: October 15, 2013
Publishe.d online:

[1] K. Autumn, N. Gravish, *Philos. Trans. Roy. Soc. London Ser. A* **2008**, *366*, 1575.
[2] K. Autumn, *Biological adhesives*, Springer Berlin Heidelberg, Germany **2006**, Ch.12.
[3] B. Bhushan, R. A. Sayer, *Applied scanning probe methods VII-Biomimetics and industrial applications*, Springer, Heidelberg, Germany **2007**.
[4] K. Autumn, Y. A. Liang, S. T. Hsieh, W Zesch, W. P. Chan, T. W. Kenny, R. Fearing, R. J. Full, *Nature* **2000**, *405*, 681.
[5] A. Peattie, C Majidi, A Corder, *J. R. Soc. Interface* **2007**, *4*, 1071.
[6] K. Autumn, C. Majidi, R. E. Groff, A. Dittmore, R. Fearing, *J. Exp. Biol.* **2006**, *209*, 3558.
[7] B. N. J. Persson, O. Albohr, U. Tartaglino, A. I. Volokitin, E. Tosatti, *J. Phys.: Condens. Matter.* **2005**, *17*, R1.
[8] K. Autumn, A. M. Peattie, *Integr. Comp. Biol.* **2002**, *42*, 1081.
[9] K. Autumn, M. Sitti, Y. A. Liang, A. M. Peattie, W. R. Hansen, S. Sponberg, T. W. Kenny, R. S. Fearing, J. N. Israelachvili, R. J. Full, *Proc. Natl. Acad. Sci. USA* **2002**, *99*, 12252.
[10] K. Autumn, A. Dittmore, D. Santos, M. Spenko and M. Cutkosky, *J. Exp. Biol.* **2006**, *209*, 3569.
[11] W. Federle, *J. Exp. Biol.* **2006**, *209*, 2611.
[12] C. Greiner, E. Arzt, A. del Campo, *Adv. Mater.* **2009**, *21*, 479.
[13] A. del Campo, C. Greiner, E. Arzt, *Langmuir* **2007**, *23*, 10235.
[14] A. K. Geim, S. V. Dubonos, I. V. Grigorieva, K. S. Novoselov, A. A. Zhukov, S. Y. Shapoval, *Nature Mater.* **2003**, *2*, 461.
[15] C. Majidi, R. E. Groff, Y. Maeno, B. Schubert, S. Baek, B. Bush, R. Maboudian, N. Gravish, M. Wilkinson, K. Autumn, R. S. Fearing, *Phys. Rev. Lett.* **2006**, *97*, 76103.
[16] H. E. Jeong, J. K. Lee, H. N. Kim, S. H. Moon, K. Y. Suh, *Proc. Natl. Acad. Sci. USA* **2009**, *106*, 5639.
[17] M. P. Murphy, S. Kim, M. Sitti, *ACS Appl. Mater. Interfaces* **2009**, *1*, 849–855.
[18] K. Y. Suh, H. E. Jeong, D.-H. Kim, R. A. Singh, E.-S. Yoon, *J. Appl. Phys.* **2006**, *100*, 034303.
[19] T. Kim, H. E. Jeong, K. Y. Suh, H. H. Lee, *Adv. Mater.* **2009**, *21*, 2276.
[20] A. Y. Y. Ho, L. P. Yeo, Y. C. Lam, I. Rodriguez, *ACS Nano* **2011**, *5*, 1897.
[21] L. Qu, L. Dai, *Adv. Mater.* **2007**, *19*, 3844.
[22] L. Ge, S. Sethi, L. Ci, P. Ajayan, A. Dhinojwala, *Proc. Natl. Acad. Sci. USA* **2007**, *104*, 10792.
[23] S. Sethi, L. H. Ge, L. J. Ci, P. M. Ajayan, A. Dhinojwala, *Nano Lett.* **2008**, *8*, 822.
[24] B. Chen, P. G. Oppenheimer, T. A. V. Shean, C. T. Wirth, S. Hofmann, J. Robertson, *J. Phys. Chem. C* **2012**, *116*, 20047.
[25] C. T. Wirth, S. Hofmann, J. Robertson, *Diamond Relat. Mater.* **2008**, *17*, 1518.
[26] C. Greiner, E. Arzt, A. del Campo, *Adv. Mater.* **2009**, *21*, 479.
[27] A. del Campo, E. Arzt, *Macromol. Biosci.* **2007**, *7*, 118.
[28] L. Qu, L. Dai, M. Stone, Z. Xia, Z. Wang, *Science* **2008**, *322*, 238.
[29] Y. Maeno, Y. Nakayama, *Appl. Phys. Lett.* **2009**, *94*, 012103.
[30] P. G. Oppenheimer, T. Hutter, B. Chen, J. Robertson, S. Hofmann, S. Mahajan, *J. Phys. Chem. Lett.* **2012**, *23*, 3486.
[31] G. Zhong, J. H. Warner, M. Fouquet, A. W. Robertson, B. Chen, J. Robertson, *ACS Nano* **2012**, *6*, 2893.
[32] J. H. Dirks, C. J. Clemente, W. Federle, *J. R. Soc. Interface* **2010**, *7*, 587.
[33] D. Sameoto, C. Menon, *Smart Mater. Struct.* **2010**, *19*, 103001.
[34] J. Lee, C. Majidi, B. Schubert, R. S. Fearing, *J. R. Soc. Interface* **2008**, *5*, 835.
[35] M. P. Murphy, B. Aksak, M. Sitti, *Small* **2009**, *5*, 170.
[36] S. Vajpayee, R. Long, L. Shen, A. Jagota, C. Y. Hui, *Langmuir* **2009**, *25*, 2765.
[37] M. D. Bartlett, A. B. Croll, D. R. King, B. M. Paret, D. J. Irschick, A. J. Crosby, *Adv. Mater.* **2012**, *24*, 1078.
[38] C. Greiner, A. del Campo, E. Arzt, *Langmuir* **2007**, *23*, 3495.
[39] G. Huber, S. N. Gorb, N. Hosoda, R. Spolenak, E. Arzt, *Acta Biomater.* **2007**, *3*, 607.
[40] J. Yu, S. Chary, S. Das, J. Tamelier, K. L. Turner, J. N. Israelachvili, *Langmuir* **2012**, *28*, 11527.
[41] B. Aksak, M. P. Murphy, M. Sitti, 2008 IEEE Int. Conf. on Robotics and Automation, Pasadena, CA, USA, May 19–23, **2008**.
[42] B. Schubert, J. Lee, C. Majidi, R. S. Fearing, *J. R. Soc. Interface* **2008**, *5*, 845.
[43] C. S. Majidi, R. E. Groff, R. S. Fearing, *J. Appl. Phys.* **2005**, *98*, 103521.
[44] R. Spolenak, S. Gorb, E. Arzt, *Acta Biomater.* **2005**, *1*, 5.
[45] B. N. J. Persson, *J. Chem. Phys.* **2003**, *118*, 7614.
[46] C. Mattevi, C. T. Wirth, S. Hofmann, R. Blume, M. Cantoro, C. Ducati, C. Cepek, A. Knop-Gericke, S. Milne, C. Castellarin-Cudia, S. Dolaf, A. Goldoni, R. Schloegl, J. Robertson, *J. Phys. Chem. C* **2008**, *112*, 12207.